J. Fluid Mech. (1996), *vol.* 320, *pp.* 53 69

Turbulence characteristics of a boundary layer over a two-dimensional bump

By D. R. WEBSTER†, D. B. DEGRAAFF AND J. K. EATON

Thermosciences Division, Department of Mechanical Engineering, Stanford University, Stanford, CA 94305-3030, USA

(Received 29 September 1995 and in revised form 15 March 1996)

The turbulent flow development was examined for a two-dimensional boundary layer over a bump. The upstream boundary layer had a momentum-thickness Reynolds number of approximately 4030. The ratios of upstream boundary layer thickness to bump height and convex radius of curvature were 1.5 and 0.06, respectively. The bump was defined by three tangential circular arcs, which subjected the flow to alternating signs of pressure gradient and surface curvature. The boundary layer grew rapidly on the downstream side of the bump but did not separate. The mean velocity profiles deviated significantly from the law of the wall above the bump. The change from concave to convex surface curvature near the leading edge triggered an internal boundary layer, as shown by knee points in the turbulent stress profiles. The internal layer grew rapidly away from the wall on the downstream side of the bump owing to the adverse pressure gradient. The effect of convex surface curvature was considered small since the flow behaviour was generally explained by the effects due to streamwise pressure gradient. A second internal layer was triggered by the change from convex to concave curvature near the trailing edge. The boundary layer recovered rapidly in the downstream section and approached typical flat-plate boundary layer behaviour at the last measurement location.

1. Introduction

The effects of various simple perturbations on two-dimensional turbulent boundary layers have been explored thoroughly. There is now a good understanding of the effects of longitudinal surface curvature, streamwise pressure gradient, surface roughness, and lateral strain when they act independently. Most practical engineering flows involve combinations and abrupt changes of these idealized perturbations. Unfortunately, there is no evidence that the response of the boundary layer to a series of perturbations is a simple superposition of the responses to independent perturbations. Generally, when there is a sudden change in the boundary conditions, such as a change in the pressure gradient or surface curvature, the boundary layer responds by forming an internal layer that grows from the wall. Smits & Wood (1985) note that the inner layer forms owing to a mismatch between the shear stress near the wall and that dictated by law-of-the-wall behaviour. The outer layer retains its previous structure until the inner boundary layer grows through it, which often results in very slow recovery of the outer layer. While this general description of boundary layer response to a discontinuity in boundary conditions is well established, the detailed effects of a series of simple

† Present address: Department of Aerospace Engineering and Mechanics, University of Minnesota, Minneapolis, MN 55455, USA.

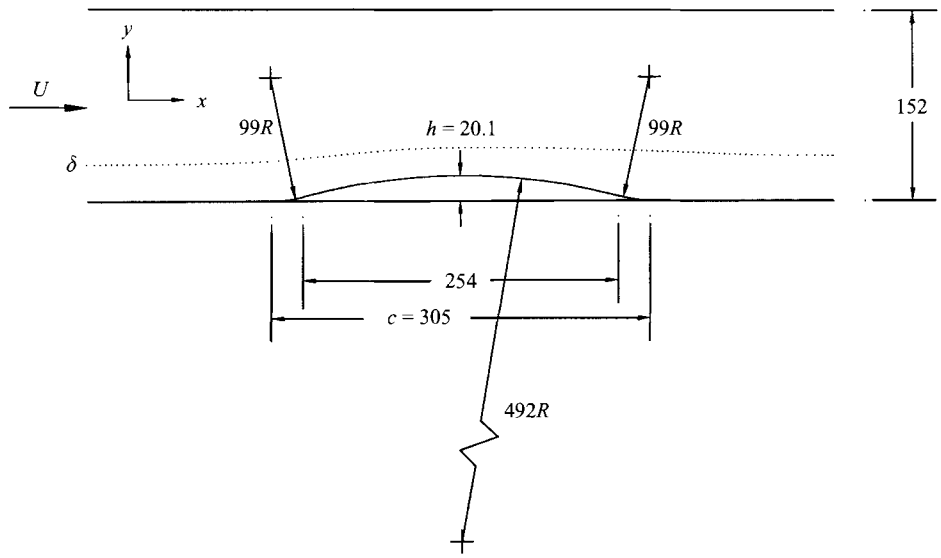

FIGURE 1. Sketch of test-section and bump geometry. All dimensions in millimetres.

perturbations have been investigated in only a few previous experiments. There is a need for more experiments which document the boundary layer under these conditions.

In this paper we present experimental results from a turbulent boundary layer flowing over a surface bump which provided significant surface curvature and streamwise pressure gradient effects. The bump profile is shown in figure 1 and was defined by three tangential circular arcs arranged such that the leading and trailing edges were tangent to the tunnel floor. The boundary layer experienced a short concave region, a longer convex region, another short concave region, and then returned to the flat plate. The flow was also subjected to streamwise pressure gradients: first mild adverse, then strong favourable, strong adverse, and finally mild favourable. The ratio of the initial boundary layer thickness to bump height (δ/h) was 1.5, and the ratio of boundary layer thickness to convex radius of curvature (δ/R) was 0.06. The boundary layer grew rapidly on the downstream side of the bump but did not separate.

Tsuji & Morikawa (1976) have examined the particular case of a turbulent boundary layer exposed to alternating signs of pressure gradient: specifically zero to adverse, to favourable, to adverse, and finally to favourable. The perturbation was sufficient to cause the disappearance of the logarithmic layer after the first adverse and favourable pressure gradient regions. An internal layer was observed in the second adverse pressure gradient region. The thickness of the internal layer was shown by knee points in the turbulent shear stress profiles. The shear stress changed due to changes in pressure gradient in the internal layer while it was conserved along streamlines above. The turbulent boundary layer over a bump examined in the current study was subjected to a similar alternating pressure gradient; however, the complexity was increased by the addition of surface curvature.

A similar flow geometry to ours was examined by Baskaran, Smits & Joubert (1987, 1991). In that experiment δ/h was 0.25, δ/R was 0.05, and the flow separated from the downstream side of the 'hill'. The authors observed an internal boundary layer that grew in the convex region of the hill and was triggered by the abrupt change in surface curvature from concave to convex. The internal layer was again shown by knee points in the turbulent stress profiles. Once formed, the internal layer developed almost

independently of the shrouding external free turbulence layer and dictated the turbulence behaviour and skin friction. The external free turbulence layer qualitatively behaved like a free turbulent flow affected by a wall constraint. In the convex region, the knee points moved away from the wall. Below the knee points the turbulent stresses increased as the internal layer grew away from the wall, which was consistent with the effect due to pressure gradient. In the external layer, the turbulent stresses decreased slowly due to prolonged convex streamline curvature.

The effect of convex surface curvature has been examined by several authors including So & Mellor (1973), Smits, Young & Bradshaw (1979), Gillis & Johnston (1983), Muck, Hoffmann & Bradshaw (1985) and Alving, Smits & Watmuff (1990). Gillis & Johnston (1983) observed an immediate reduction of the turbulent mixing length in response to the surface curvature. An 'active' shear stress internal layer was formed, while the turbulent shear stress in the outer layer decreased to nearly zero. The internal layer dominated the turbulence dynamics and its thickness scaled the turbulent mixing length. Alving *et al.* (1990) verified their observation that the recovery was very slow downstream of the curved surface section, especially beyond ten boundary layer thicknesses. Turbulent flows respond to concave surface curvature more slowly and the dynamics are dominated by large-scale streamwise-aligned vortices which are analogous to Taylor–Görtler vortices (Barlow & Johnston 1988). Baskaran *et al.* (1987) found no evidence of Taylor–Görtler-like streamwise vortices in the short concave surface sections of their hill flow.

In an attempt to utilize the asymmetric response to concave and convex surfaces, Bandyopadhyay & Ahmed (1993) showed that the flow over a flat to concave to convex to flat wall had a sustained lower value of skin friction than the flat to convex to concave to flat case. They observed internal layers growing from each discontinuity in surface curvature. In regions of concave curvature the outer-layer turbulence intensity was amplified while in the convex surface regions it was suppressed.

The current flow configuration had two discontinuities in surface curvature: concave to convex near the leading edge and convex to concave near the trailing edge. Baskaran *et al.* (1987) established a surface curvature discontinuity criterion of $\Delta k^* = (1/R_2 - 1/R_1)\,\nu/u_{\tau 0} > 0.37 \times 10^{-4}$ (where R_1 and R_2 are upstream and downstream radii of curvature and $u_{\tau 0}$ is the friction velocity on the upstream side) for the formation of internal layers. The current flow had $\Delta k^* = 2.9 \times 10^{-4}$ at both discontinuities. Hence, the first discontinuity was expected to trigger an internal layer which would grow over the convex surface. Since the flow did not separate, the second discontinuity should trigger a second internal layer which would grow on the downstream flat plate. Baskaran *et al.* (1987, 1991) did not observe this second internal layer since their flow separated before the discontinuity of surface curvature.

The objective of this paper is to report the detailed response of a turbulent boundary layer to a series of simple perturbations. Mean velocity and turbulent characteristics are reported at several locations on the downstream side and recovery region of the two-dimensional bump. The complex interaction of the surface curvature and streamwise pressure gradient effects is discussed.

2. Facility and experimental techniques

The experiments were performed in a low-speed, blower-driven wind tunnel with a 152 by 711 mm rectangular test section. All data reported in this paper correspond to a nominal velocity of 16.6 m s^{-1} and a free-stream turbulence intensity of 0.2% at the first measurement location. All measurements were performed in the tunnel-floor

boundary layer which was tripped 150 mm downstream of the test section inlet and developed for 1.8 m upstream of the bump. The dimensions of the test section and bump profile are shown in figure 1. The solid aluminium bump model was bolted to the tunnel floor. All reported measurements are in the tunnel coordinate system, such that x, y and z are the free-stream, wall-normal and spanwise directions, respectively. A second normalized streamwise coordinate, $x' = (x - x_0)/c$, is also used, where x_0 corresponds to the leading edge of the bump and c is the bump chord length. In the x'-coordinate system, zero is the leading edge, 0.5 is the bump apex and 1.0 is the trailing edge. The zero location for the y-axis is shifted to correspond to the surface location. The y-axis is also maintained normal to the flat plate at locations above the bump because the initial boundary layer thickness was greater than the bump height, and there was very little streamline curvature in the outer layer.

Wall static pressure data were measured through 0.635 mm diameter surface pressure taps (spaced at 25.4 mm intervals) using a Setra differential pressure transducer (model 239, ± 2.5 in. H_2O range). The static pressure measurements showed that the streamwise pressure gradient was too large for reliable Preston tube measurements as determined by Patel (1965) and others. Attempts to infer the shear stress from the Clauser chart verified that the profiles had deviated significantly from typical logarithmic layer behaviour. As a result, the wall skin friction was measured with an oil flow fringe imaging technique (Monson, Mateer & Menter 1993) that relies on the proportionality of the oil film thickness to the wall shear. To utilize this method, the surface of the tunnel floor and bump model were covered with a 0.08 mm thick self-adhering mylar sheet in order to provide a black background for the imaging. Dow Corning Fluid 200 with 50 cS viscosity was used. An in-tunnel calibration station was located upstream of the bump at location $x' = -0.33$. Ten independent measurements were collected at each streamwise location and averaged. The measurements showed good repeatability and the uncertainty was estimated to be $\pm 5\%$ of the reference value.

All reported velocity measurements were performed on the tunnel centreline and limited measurements were collected at other spanwise locations (specifically at $z = \pm 25.4$ mm and ± 50.8 mm relative to the centreline) in order to verify spanwise uniformity. The velocity measurements were performed with the single-wire and cross-wire probes described in Littell & Eaton (1994). The probes used 2.5 μm platinum-coated tungsten wire which was copper plated and then etched for an active length-to-diameter ratio of 250. The active length was $l^+ = 30$ at the location $x' = -0.33$. The cross-wires were separated by 0.35 mm and could be rotated about their axes in 45° increments, allowing measurements of all six Reynolds stresses. The data were measured with a TSI constant-temperature anemometer (model IFA-100) operating at a resistance ratio of 1.8. The voltage signal was DC shifted and amplified and then filtered at 10 kHz. At each location 5000 samples were collected at 250 Hz. The probe was calibrated in the tunnel using King's law before every profile acquisition. The air temperature was measured before data acquisition at every point and the Bearman (1971) temperature correction was applied to the measured hot-wire voltage. The effective wire angles were found by assuming cosine response and following the calibration yawing procedure described in Westphal & Mehta (1984).

The probes were positioned using a two-axis traverse which had resolution of 0.0015 mm and 0.003 mm in the vertical and streamwise directions, respectively. The initial vertical position of the probes was set by observing the electrical contact resistance between the probe prongs (an attached post was used for the x-wire probe) and the conducting floor of the test section. The data acquisition was performed with

a 486 PC clone and National Instruments AT-MIO-16 (12-bit A/D) and GPIB-PCII boards. An external simultaneous sample and hold circuit was used to collect the x-wire voltages. The computer was also used to control the tunnel speed and traverse movement.

Following the analysis of Anderson & Eaton (1989) the following uncertainties have been estimated for the hot-wire measurements. The mean velocities had an uncertainty of $\pm 3\%$ of the local streamwise velocity. The normal Reynolds stress components had an uncertainty of $\pm 5\%$ of the local value of $\overline{u'^2}$. The shear stress had an uncertainty of $\pm 10\%$ of the local value of $\overline{u'v'}$. Sample error bars are shown on the mean velocity and Reynolds stress profiles. Typically, the repeatability and the agreement between the single-wire and cross-wire measurements was better than the theoretically estimated uncertainty ($\pm 1\%$ for the mean velocity components and $\pm 3\%$ for the Reynolds stress quantities).

3. Results and discussion

The static pressure distribution is shown in figure 2(*a*) non-dimensionalized by the dynamic pressure at the upstream reference location ($x' = -0.33$): $C_p = (P_{static} - P_{ref})/\frac{1}{2}\rho U_{ref}^2$. As discussed in the introduction, the flow encountered a mild adverse pressure gradient as it approached the bump. The flow accelerated in a strong favourable pressure gradient on the upstream side of the bump and then decelerated in the similarly strong adverse pressure gradient on the downstream side. Downstream of the bump was a constant-area rectangular test section and the flow relaxed back to a near-zero pressure gradient.

The skin friction coefficient, $C_f = \tau_w/\frac{1}{2}\rho U_{ref}^2$, is shown in figure 2(*b*). The shear stress upstream of the bump decreased due to the mild adverse pressure gradient. Above the bump, the shear stress distribution generally followed the pressure gradient: increasing rapidly in the favourable pressure gradient, and decreasing in the adverse pressure gradient. The slight dip centred near the bump apex ($x' = 0.5$) was clearly evident in all independent measurements. This probably resulted from the early stages of relaminarization. The initial rapid increase in skin friction is interrupted when relaminarization suppresses the turbulent fluctuations (see, for example, Badri Narayanan & Ramjee 1969). As the flow approached the trailing edge of the bump, the skin friction decreased rapidly. The use of tufts failed to identify any recirculation zone and the surface oil flow was consistently in the free-stream direction, indicating that the flow did not separate. Downstream of the bump, the skin friction gradually increased in the mildly favourable pressure gradient.

Hot-wire measurements were performed at the upstream reference location ($x' = -0.33$) and at nine locations between the bump apex ($x' = 0.5$) and downstream of the bump at $x' = 1.67$. Measurements were collected for three reference location momentum thickness Reynolds numbers roughly equal to 1500, 2500 and 4000. The behaviour was similar for each case and only the largest Re is presented and discussed here. Table 1 shows the local external velocity, U_e; the displacement thickness, δ^*; the momentum thickness, θ; the shape factor, H, and the momentum-thickness Reynolds number, Re_θ. The local external velocity increased by approximately 15% between the upstream reference location and the bump apex owing to the tunnel area reduction. On the downstream side of the bump, the external velocity decreased in the adverse pressure gradient and then increased slightly in the downstream recovery. The boundary layer was thinned significantly (approximately 30% reduction in momentum thickness) at the bump apex owing to the acceleration. The momentum thickness

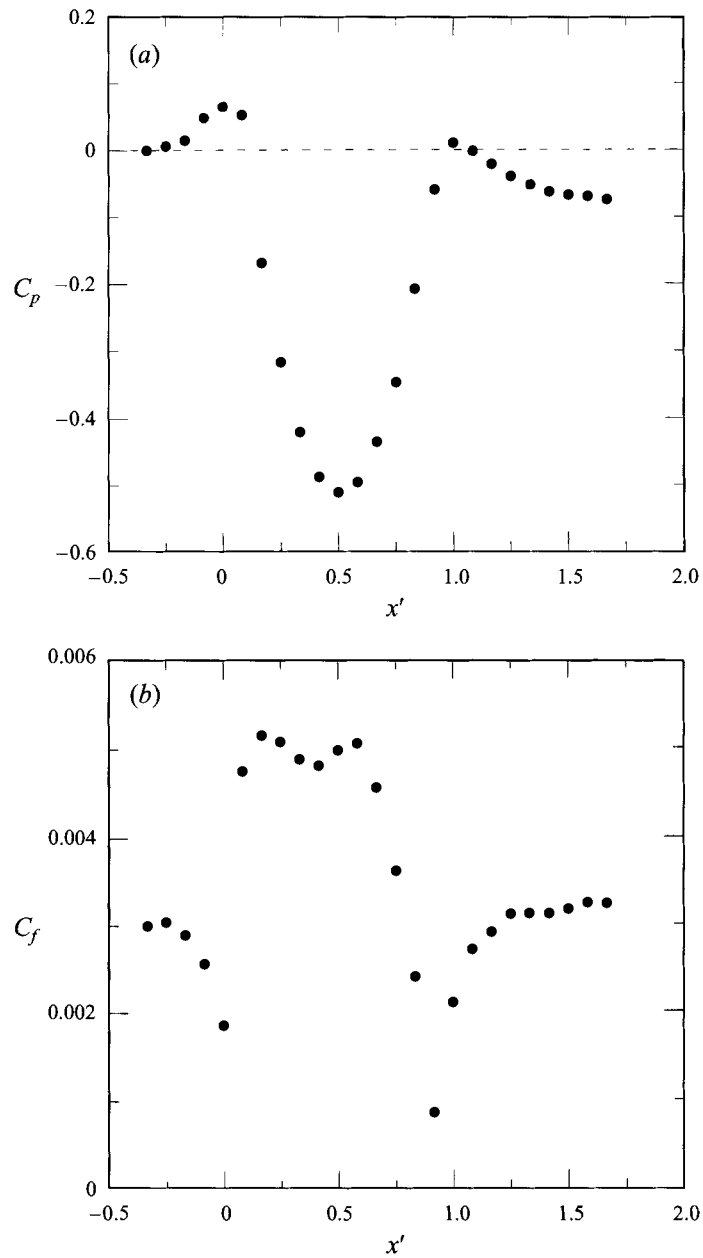

FIGURE 2. (*a*) Static pressure coefficient. (*b*) Skin friction coefficient.

increased by more than 100% between the bump apex and trailing edge. The profiles of mean velocity and turbulent stresses presented in this paper have been normalized by the local external velocity. This normalization masks the acceleration but provides ready comparison between profiles at the various locations. The vertical coordinate has been normalized by the local momentum thickness which masks the thinning and growth of the layer, but again provides ready relative comparison between stations.

The u-component mean velocity is shown in semi-logarithmic form in figure 3. The profile at $x' = -0.33$ shows a well-defined logarithmic layer and agrees very well with

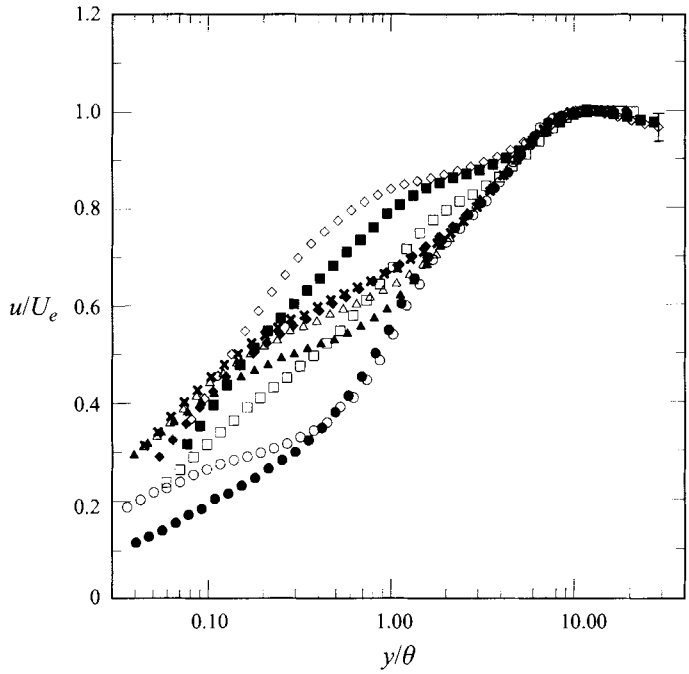

FIGURE 3. Mean u-velocity profiles for various x'; for symbols see table 1.

x'	U_e (m s^{-1})	δ^* (mm)	θ (mm)	H	Re_θ	Symbol
−0.33	16.6	5.09	3.67	1.39	4030	◆
0.5	19.2	2.93	2.46	1.19	3070	◇
0.67	18.8	3.24	2.60	1.25	3170	■
0.83	17.8	4.72	3.35	1.41	3930	□
0.92	17.5	8.09	4.96	1.63	5650	●
1.0	17.0	9.00	5.51	1.63	6130	○
1.17	16.7	7.30	5.04	1.45	5510	▲
1.33	16.8	6.32	4.49	1.41	4960	△
1.5	16.9	6.13	4.42	1.39	4940	★
1.67	16.9	6.12	4.44	1.38	4890	✖

TABLE 1. Integral parameters at profile locations

the law of the wall (not shown). The profiles above the bump show significant distortion from the typical logarithmic layer. The profile at $x' = 0.5$ has the typical shape previously observed in the early stages of relaminarization (again see Badri Narayanan & Ramjee 1969). On the upstream side of the bump the acceleration parameter, $\Delta_p = -\nu(\mathrm{d}p/\mathrm{d}x)/\rho u_\tau^3$, reached a peak value of 0.025, thus exceeding the value of 0.018 set by Patel (1965) to denote major departures from the logarithmic layer. It should be noted that the acceleration parameter based on free-stream variables, $K = \nu(\mathrm{d}U_e/\mathrm{d}x)/U_e^2$, reached a peak value of approximately 8×10^{-7} which is generally considered insufficient to relaminarize. However, this parameter contains no information about the inner region of the boundary layer which is crucial in this flow. On the downstream side of the bump, the profiles show a large velocity deficit region near the wall, as expected in an adverse pressure gradient. In the downstream region the flow relaxes back to the typical flat-plate boundary layer shape; the last location

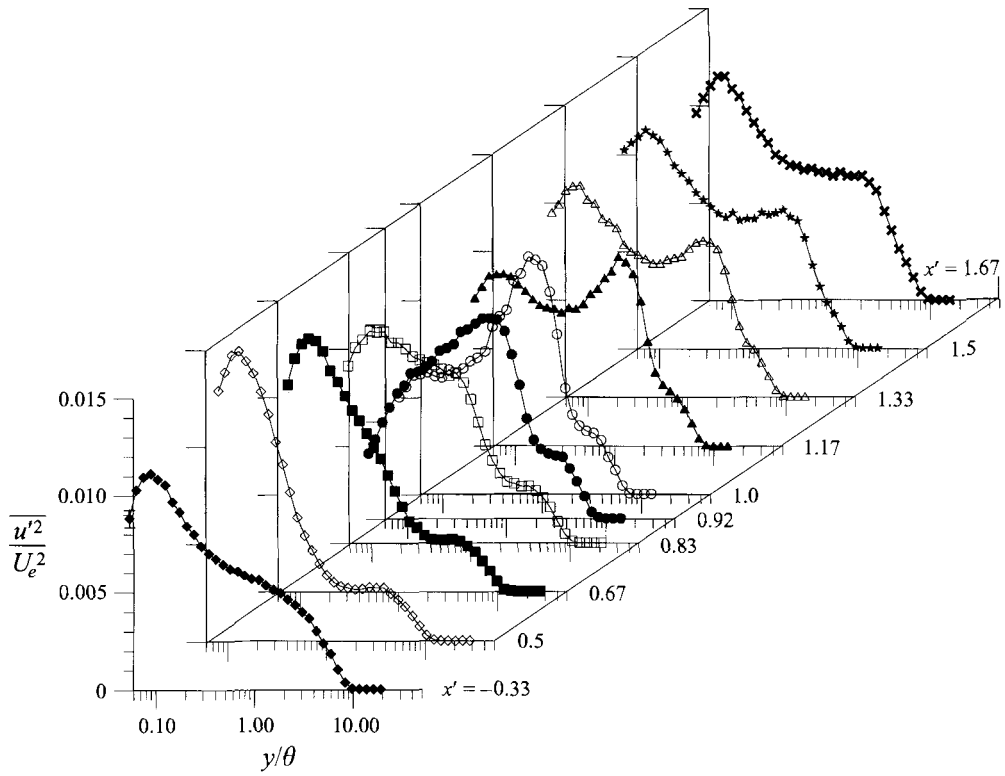

FIGURE 4. Profiles of $\overline{u'^2}$. For symbols see table 1.

($x' = 1.67$) shows only slight differences with the upstream reference profile. This quick recovery of the logarithmic layer is in agreement with the study of Tsuji & Morikawa (1976).

The v-component mean velocity is not shown here. At measurement locations above the flat plate (upstream and in the recovery region) the vertical velocity was near zero. The vertical velocity was directed downward on the downstream side of the bump, and reached a measured maximum of approximately $-0.12U_e$ at $x' = 0.83$. The measured w-component mean velocity was zero everywhere to well within the experimental uncertainty. This fact supports the assertion that Taylor–Görtler-like vortex structures were not formed over the short concave surface curvature region. Further support was found in the limited profiles taken at off-centreline locations which showed no variation across the middle third of the tunnel. Skin friction measurements also were performed at closely spaced spanwise positions, and showed no significant variability.

The profiles of the streamwise turbulent normal stress, $\overline{u'^2}$, are shown in figure 4. The profiles are shown on identical axes, staggered in order to clearly see the evolution of the flow. The upstream reference profile shows good agreement with that observed in the previous investigations (e.g. Erm & Joubert 1991). At the bump apex, the profile has a knee point at approximately $y/\theta = 1$ which indicates that an internal layer had been triggered by the discontinuity in surface curvature at $x' = 0.08$. Below the knee point, the normal stress is greater than the upstream reference value, while it is less in the outer layer owing to the favourable pressure gradient. In the profiles on the downstream side of the bump, the knee point and the location of the local maximum moves away from the wall, indicating that the internal layer grows away from the wall in the adverse pressure gradient. By the $x' = 1.0$ location the internal layer had grown

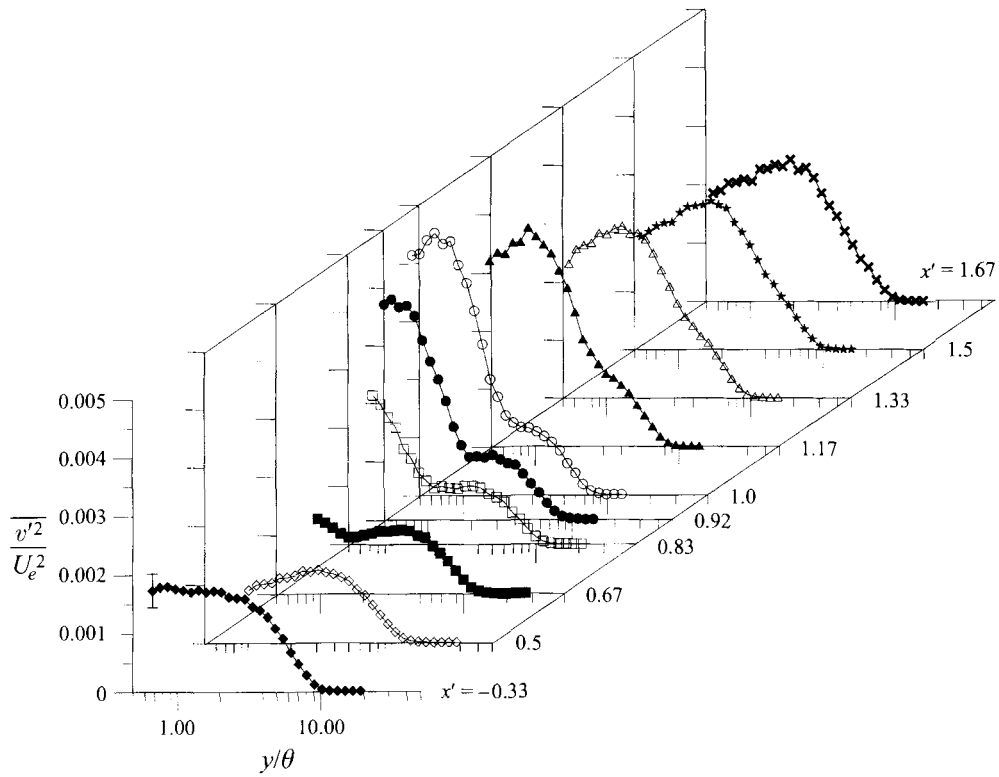

FIGURE 5. Profiles of $\overline{v'^2}$. For symbols see table 1.

to approximately $y/\theta = 3$ while the momentum thickness had also grown significantly. The peak value of $\overline{u'^2}$ deceased in dimensional terms in this region since the normalizing external velocity was also decreasing.

The flow encountered a second discontinuity in surface curvature at $x' = 0.92$, which triggered a second internal layer. The first evidence of this is at the $x' = 1.17$ location where two local maxima in the $\overline{u'^2}$ profile are observed. The inner peak is due to the new internal layer and the outer peak is the remnants of the upstream internal layer. As the flow evolves downstream on the flat plate, the new internal layer grows while the outer peak decays away. The resulting profile at $x' = 1.67$ is very similar to the upstream reference although at slightly elevated values.

The profiles of the other normal stresses, $\overline{v'^2}$ and $\overline{w'^2}$, $\overline{q^2}(= \overline{u'^2}+\overline{v'^2}+\overline{w'^2})$, and the shear stress, $\overline{u'v'}$ are shown in figures 5–8, respectively. It should be noted that the abscissa is different in these figures from that in figure 4 because the cross-wire probe could not measure as close to the wall as the single-wire probe. In each case the upstream reference location profile agrees well with the typical flat-plate behaviour observed in previous investigations. These quantities qualitatively followed the evolution of $\overline{u'^2}$ discussed above. The growth of the first inner layer can be seen in the profiles on the downstream side of the bump. The remnants of the first internal layer decay away in the downstream recovery region. The x-wire used to measure these quantities did not provide sufficient resolution near the wall to observe the second internal layer. By the last station each profile resembles the upstream reference, although it has slightly larger normalized values. Also shown on the ordinate for each profile in figure 8 is the skin friction measurement normalized by the local external

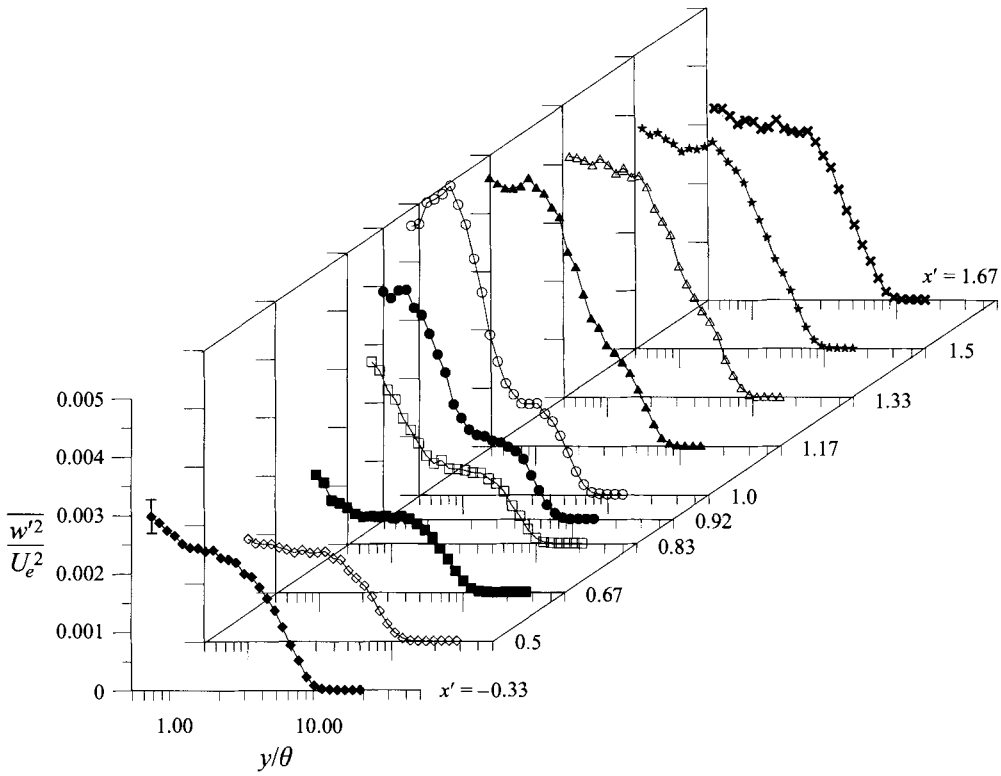

FIGURE 6. Profiles of $\overline{w'^2}$. For symbols see table 1.

velocity. The skin friction data are consistent with the $\overline{u'v'}$ profiles and behaviour described above. The profiles of $\overline{u'w'}$ are not shown here since they were uniformly zero to within the stated uncertainty. The profiles of $\overline{v'w'}$ were not measured (except at the upstream reference) and were assumed to be zero.

In all of the turbulent stress plots, the profiles beyond approximately $y/\theta = 4$ show only mild variation. The u-component mean velocity profiles in figure 3 also show similarity at all locations for $y/\theta > 4$. This indicates that the outer region of the boundary layer was relatively unaffected by the surface bump. Gillis & Johnston (1983) and others have shown a rapid decrease in the turbulent shear stress in the outer layer for the convex surface curvature flow. In the hill flow, Baskaran *et al.* (1987) noted a gradual decrease of the turbulent stresses in this outer region owing to prolonged streamline curvature. The relatively small impact on the outer layer in the current flow indicates that the effect of streamline curvature was mild in that region.

Figure 9 shows selected profiles of the anisotropy parameter, $\overline{v'^2}/\overline{u'^2}$. Gillis & Johnston (1983) noted that the turbulence was nearly isotropic (i.e. $\overline{u'^2} = \overline{v'^2} = \overline{w'^2}$, $\overline{u'v'} = 0$) in the outer layer of their boundary layer on a convex surface. In the convex surface region of the hill flow, Baskaran *et al.* (1991) found that the turbulence was anisotropic and furthermore that $\overline{v'^2}$ decreased more rapidly than $\overline{u'^2}$ owing to the addition of a streamwise pressure gradient. In the current flow, the anisotropy parameter profile at the upstream reference is in the range of 0.3 to 0.4 across most of the boundary layer. The parameter is slightly larger at the bump apex and slightly smaller on the downstream side of the bump. In the downstream recovery region the profiles are nearly identical to the reference one. Profiles of $\overline{w'^2}/\overline{u'^2}$, although not shown here, revealed essentially the same behaviour. It is apparent that the normal stresses

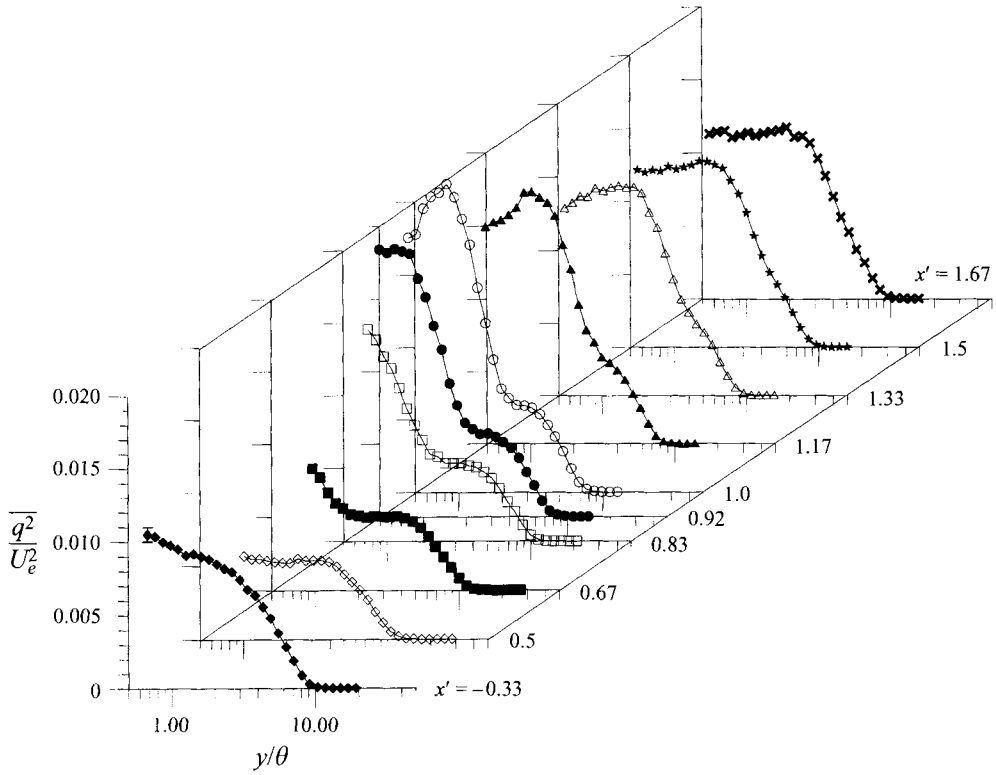

FIGURE 7. Profiles of $\overline{q^2}$. For symbols see table 1.

were responding to the bump nearly identically since there was only slight deviation from the flat-plate ratio. Furthermore, the results indicate that the streamline curvature effect was small in comparison to Baskaran *et al.* (1991) and Gillis & Johnston (1983).

Figure 10 shows the profiles of the Townsend structure parameter, $A_1 = \overline{u'v'}/\overline{q^2}$. The measured profiles were mildly smoothed in the y-direction before calculating the quantities in figures 10 and 11 only. The smoothing procedure used a weighted average of each datum with its two neighbouring points. The upstream reference profile has the typical flat-plate boundary layer shape and a value of approximately 0.14 across the layer. All of the profiles show near similarity for y/θ greater than 4, while the value closer to the wall varies significantly. At the bump apex, A_1 near the wall is about 0.09. On the downstream side of the bump where the internal layer was growing from the wall A_1 grows to a peak value of nearly 0.2 at $x' = 0.92$ and 1.0. In the downstream recovery region A_1 relaxes to about 0.12 near the wall at the last location. The slightly low value at the last station was due to the shear stress returning to typical values before the kinetic energy level decreased (see figures 7 and 8). The behaviour of A_1 near the wall was similar to that observed throughout the boundary layer of Tsuji & Morikawa (1976). In that flow A_1 increased in the first adverse pressure gradient and decreased in the first favourable pressure gradient. In the second adverse pressure gradient, the profiles of A_1 had a nearly constant value of approximately 0.12. Gillis & Johnston (1983) showed that the A_1 parameter responded quickly to convex surface curvature and was reduced substantially in the outer layer. The A_1 profile at the apex of the hill flow of Baskaran *et al.* (1987) was similar to the $x' = 0.5$ profile here. On the downstream side of the hill, A_1 increased in the internal layer in agreement with the profiles shown here. However for the Baskaran *et al.* (1987) flow, A_1 decreased in the

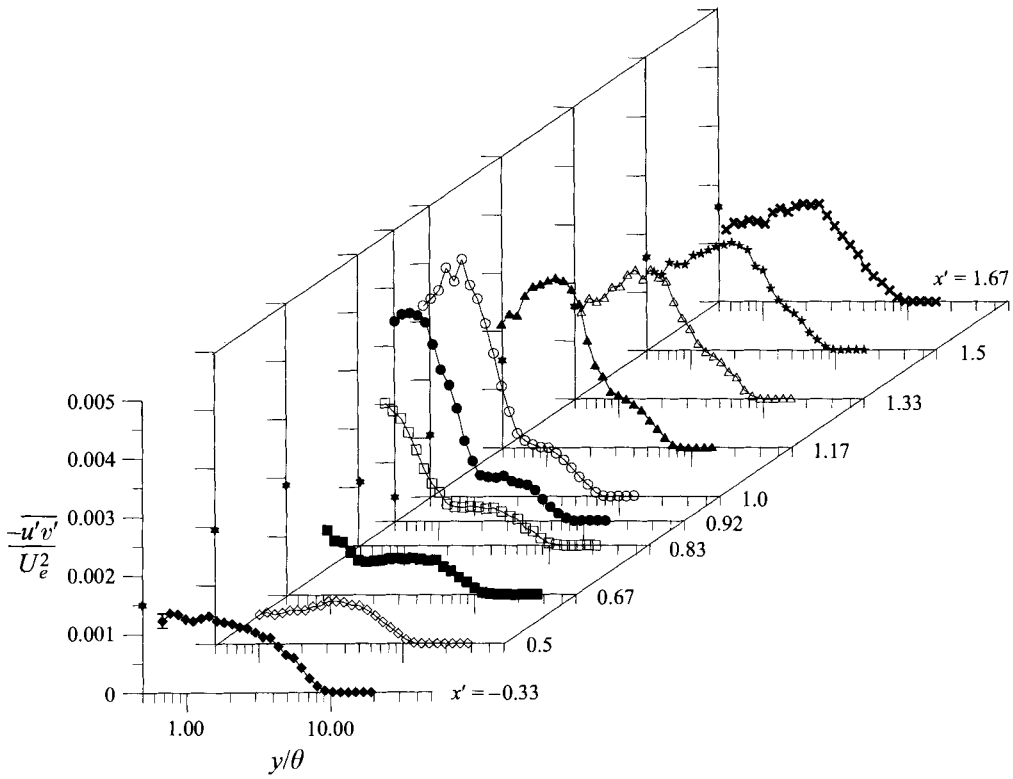

FIGURE 8. Profiles of $\overline{u'v'}$. Also shown is $C_f/2$, ✱, (based on local external velocity) on the ordinate. For symbols see table 1.

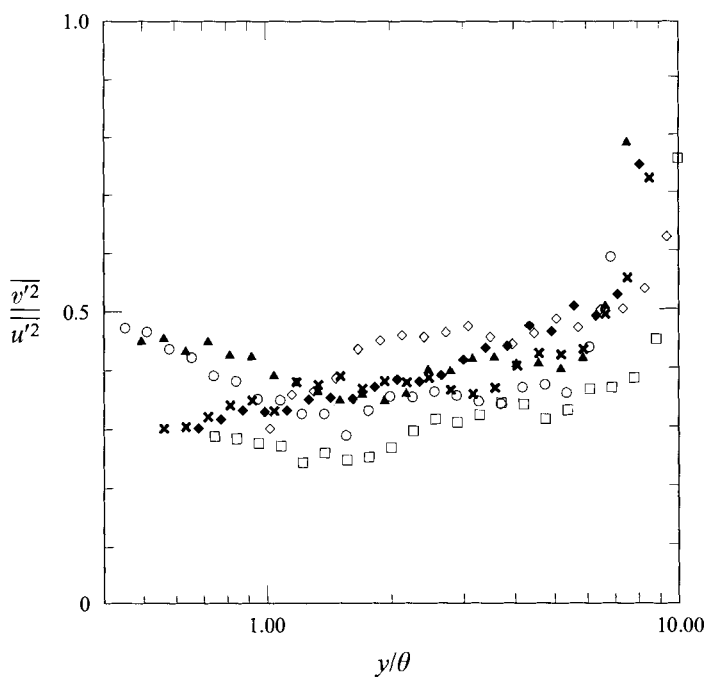

FIGURE 9. Selected profiles of the anisotropy parameter, $\overline{v'^2}/\overline{u'^2}$. For symbols see table 1.

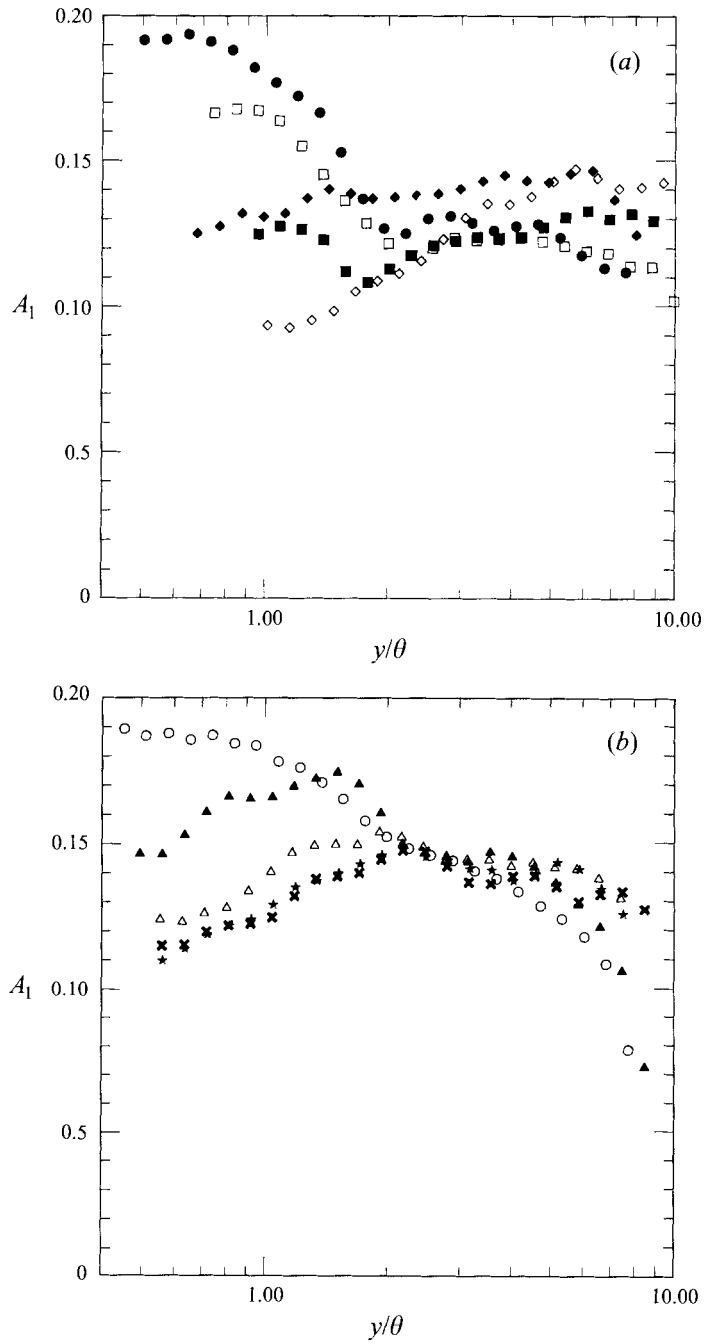

FIGURE 10 (*a*, *b*). Profiles of the Townsend structure parameter, A_1. For symbols see table 1.

outer layer owing to streamline curvature, becoming negative just before separation. The conclusion for the current flow is that the turbulent structure parameter in the internal layer was influenced by the streamwise pressure gradient, while the effect of streamline curvature in the outer layer was very mild.

Since the flow over the bump did not separate, this geometry appears to be an excellent test case for turbulence model testing and evaluation. However, any model

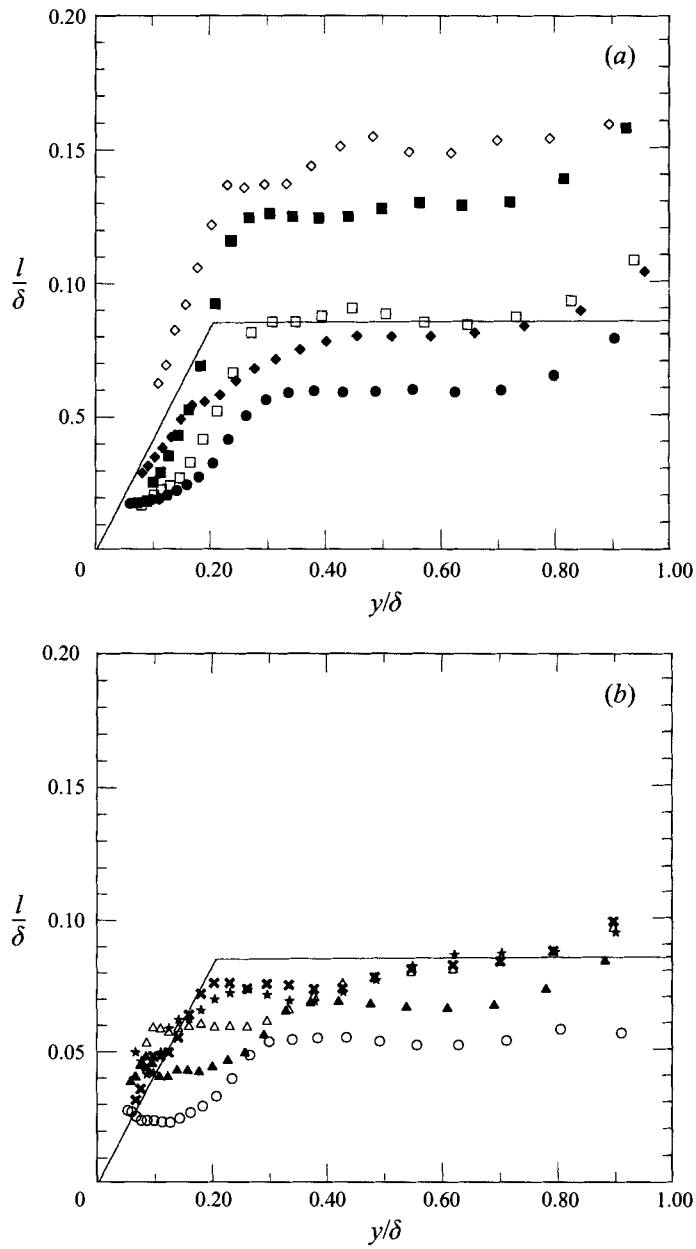

FIGURE 11 (*a*, *b*). Profiles of mixing length. For symbols see table 1.

attempting to accurately predict this flow must be robust enough to handle the complex combination of streamwise pressure gradient and surface curvature (although the former seems to dominate the physical behaviour, the abrupt changes in surface curvature lead to the formation of the internal layers). The most basic model is the Prandtl mixing length, $l = \overline{u'v'}/(\mathrm{d}u/\mathrm{d}y)$, which is shown in figure 11 normalized by the boundary layer thickness. Also shown in the figure is the standard logarithmic region correlation, $l = 0.41y$ and the constant line of $l/\delta = 0.085$. The flat-plate boundary layer profile at $x' = -0.33$ is slightly below the correlation but showed the correct qualitative behaviour. At $x' = 0.5$ and 0.67 the turbulent mixing length is significantly

larger across the profile, reaching a normalized value of approximately 0.14. The mixing length was reduced in the adverse pressure gradient, reaching a minimum of approximately 0.05 at the $x' = 1.0$ location. At this location the mixing length also deviated significantly from the standard logarithmic region correlation. In the downstream recovery, the mixing length rapidly returns to standard correlations.

The effects of the bump on the mean flow and turbulence characteristics were explained by simple streamwise pressure gradient arguments and were in qualitative agreement with the alternating pressure studied by Tsuji & Morikawa (1976). Since the predominant trends reported by Gillis & Johnston (1983) and others were not present, the effect of convex surface curvature was small. This was surprising since the curvature parameter was large, $\delta/R = 0.06$. It was also in contrast to the hill flow of Baskaran *et al.* (1987) who reported that the outer layer responded to the convex streamline curvature. The contrasting behaviour was due to the differences in flow geometry. The hill was much larger with respect to the boundary layer thickness ($\delta/h = 0.25$ for the hill and 1.5 for the current bump) and the effective angle of the convex surface region of the hill was approximately 70°, while the effective angle for the current bump flow was 30°. In the 90° bend, Gillis & Johnston (1983) found that the effet of convex wall curvature was noticeable almost immediately. However, Baskaran *et al.* (1987) observed a more gradual response to the prolonged streamline curvature. The current flow did not show the effects of the prolonged curvature because the bump caused much less flow curvature owing to the smaller height and shorter convex region. The boundary layer thickness is carefully drawn in figure 1 to illustrate this point.

The recovery of the boundary layer downstream of the bump was very rapid. The last measurement station was roughly six boundary layer thicknesses downstream of the trailing edge. At that location the mean flow profiles showed a well-defined logarithmic region, and the turbulent stress profiles showed only slightly elevated values relative to the upstream reference. The quick recovery was due to the second internal layer growing, while the remnants of the first internal layer decayed away. This process was most clearly observed in the $\overline{u'^2}$ profiles. Using flat-plate integral analysis to estimate the ideal momentum thickness with no bump yielded 4.60 mm at the $x' = 1.67$ location. This was nearly equal to the 4.44 mm measured with the bump in place. Given the significant perturbation to the flow above the bump, the rapid recovery was remarkable. The downstream flow hardly knew the bump was there.

4. Conclusions

Experimental results have been presented for a turbulent boundary layer over a surface bump. An internal layer was triggered by the discontinuity in surface curvature (concave to convex) near the bump leading edge. The boundary layer was then accelerated and subjected to convex surface curvature on the upstream side of the bump. At the bump apex the mean u-component of velocity deviated strongly from logarithmic layer behaviour, and was similar to profiles in early stages of relaminarization. The internal layer was noted in the $\overline{u'^2}$ profile by a knee point at about $y/\theta = 1$. In the region $1 < y/\theta < 4$ the turbulent stresses had been reduced substantially owing to the streamwise favourable pressure gradient. The favourable pressure gradient also had the effect of thinning the overall boundary layer significantly.

As the flow developed on the downstream side of the bump the boundary layer and the internal layer grew rapidly due to the adverse pressure gradient. The knee point in the turbulent stress profiles evolved away from the wall more rapidly than the momentum thickness, and reached a height of about $y/\theta = 3$ by the trailing edge. The

turbulent stresses appeared to be increasing on the downstream side of the bump, but this was due to the internal layer growing away from the wall. In the $\overline{u'^2}$-profiles, the magnitude in the internal layer actually decreased slightly from the magnitude at the bump apex as the internal layer grew away from the wall. While the cross-wire did not get close enough to the wall to clearly resolve the internal layer at the bump apex, the anisotropy parameter showed that the normal stress components were responding in a qualitatively similar manner. The effect of convex surface curvature was small since the predominant trends reported by Gillis & Johnston (1983) and others were not present.

The discontinuity in surface curvature near the trailing edge triggered a second internal layer which is first noted by the two maxima in the profiles of $\overline{u'^2}$ at $x' = 1.17$. The recovery to typical flat-plate boundary layer behaviour was remarkably rapid with the flow at the last measurement location strongly resembling the flow upstream of the bump.

The data are available from the authors for all three Reynolds numbers. This work was supported by the Office of Naval Research under grant number N0001494-1-0070 monitored by Dr L. P. Purtell. Thanks to Dr D. Driver at NASA-Ames for his helpful demonstration of the oil flow fringe imaging technique.

REFERENCES

ALVING, A. E., SMITS, A. J. & WATMUFF, J. H. 1990 Turbulent boundary layer relaxation from convex curvature. *J. Fluid Mech.* **211**, 529.

ANDERSON, S. D. & EATON, J. K. 1989 Reynolds stress development in pressure-driven three-dimensional turbulent boundary layers. *J. Fluid Mech.* **202**, 263.

BADRI NARAYANAN, M. A. & RAMJEE, V. 1969 On the criteria for reverse transition in a two-dimensional boundary layer flow. *J. Fluid Mech.* **35**, 225.

BANDYOPADHYAY, P. R. & AHMED, A. 1993 Turbulent boundary layers subjected to multiple curvatures and pressure gradients. *J. Fluid Mech.* **246**, 503.

BARLOW, R. S. & JOHNSTON, J. P. 1988 Structure of a turbulent boundary layer on a concave surface. *J. Fluid Mech.* **191**, 137.

BASKARAN, V., SMITS, A. J. & JOUBERT, P. N. 1987 A turbulent flow over a curved hill. Part 1. Growth of an internal boundary layer. *J. Fluid Mech.* **182**, 47.

BASKARAN, V., SMITS, A. J. & JOUBERT, P. N. 1991 A turbulent flow over a curved hill. Part 2. Effects of streamline curvature and streamwise pressure gradient. *J. Fluid Mech.* **232**, 377.

BEARMAN, P. W. 1971 Corrections for the effect of ambient temperature drift on hot-wire measurements in incompressible flow. *DISA Rep.* 11, p. 25.

ERM, L. P. & JOUBERT, P. N. 1991 Low-Reynolds-number turbulent boundary layers. *J. Fluid Mech.* **230**, 1.

GILLIS, J. C. & JOHNSTON, J. P. 1983 Turbulent boundary-layer flow and structure on a convex wall and its redevelopment on a flat wall. *J. Fluid Mech.* **135**, 123.

LITTELL, H. S. & EATON, J. K. 1994 Turbulence characteristics of the boundary layer on a rotating disk. *J. Fluid Mech.* **266**, 175.

MONSON, D. J., MATEER, G. G. & MENTER, F. R. 1993 Boundary-layer transition and global skin friction measurement with an oil-fringe imaging technique. *SAE Technical Paper Series* 932550.

MUCK, K. C., HOFFMANN, P. H. & BRADSHAW, P. 1985 The effect of convex curvature on turbulent boundary layers. *J. Fluid Mech.* **161**, 347.

PATEL, V. C. 1965 Calibration of the Preston tube and limitations on its use in pressure gradients. *J. Fluid Mech.* **23**, 185.

SMITS, A. J. & WOOD, D. H. 1985 The response of turbulent boundary layers to sudden perturbations. *Ann. Rev. Fluid Mech.* **17**, 321.

SMITS, A. J., YOUNG, S. T. B. & BRADSHAW, P. 1979 The effect of short regions of high surface curvature on turbulent boundary layers. *J. Fluid Mech.* **94**, 209.

SO, R. M. C. & MELLOR, G. L. 1973 Experiment on convex curvature effects in turbulent boundary layers. *J. Fluid Mech.* **60**, 43.

TSUJI, Y. & MORIKAWA, Y. 1976 Turbulent boundary layer with pressure gradient alternating in sign. *Aero. Q.* **27**, 15.

WESTPHAL, R. V. & MEHTA, R. D. 1984 Crossed hot-wire data acquisition and reduction system. *NASA TM* 85871.